Journal of Chromatography A, 1218 (2011) 2887–2897

Contents lists available at ScienceDirect

Journal of Chromatography A

journal homepage: www.elsevier.com/locate/chroma

Some practical comparisons of the efficiency and overloading behaviour of sub-2 μm porous and sub-3 μm shell particles in reversed-phase liquid chromatography

David V. McCalley*

Centre for Research in Biomedicine, University of the West of England, Frenchay, Bristol BS16 1QY, UK

ARTICLE INFO

Article history:
Received 28 December 2010
Received in revised form 22 February 2011
Accepted 26 February 2011
Available online 4 March 2011

Keywords:
Shell particles
Superficially porous particles
Sub-2 μm porous particles
Knox curves
Overload behaviour
UHPLC

ABSTRACT

At their optimum flow, sub-3 μm superficially porous or "shell" particles demonstrate similar efficiency to sub-2 μm totally porous particles. The performance of 0.21 cm i.d shell columns is however inferior to those of 0.46 cm i.d., presumably due to packing difficulties. At high flow, shell columns can give flatter Knox curves due to lower operating pressure (half or less of that of the totally porous particles) producing less frictional heating, which combined with the increased thermal conductivity of their non-porous core, gives more efficient heat dissipation. However, the effects of frictional heating for sub-2 μm columns are considerably exaggerated when using pure ACN as mobile phase, as it has a thermal conductivity 3 times less than that of pure water, leading to poorer heat dissipation. Overloading is already problematic for ionised solutes, a group which contains many pharmaceuticals and compounds of clinical relevance, on conventional columns (5 μm porous particles). However, it becomes a more serious issue for both new column types, partially as a result of their very high efficiency, which concentrates the sample as a very narrow band. The sample capacity of one type of shell particle was estimated to be 60% of that of the small totally porous particles, in line with the fraction of the particle volume that is porous. Due to overloading, it is barely possible to achieve perfect peak symmetry for ionised acids or bases with either of these new column types, even by injecting the lowest amounts of sample detectable by UV. While ammonium formate and potassium phosphate buffers gave similar results in overloading studies, use of formic acid as sole mobile phase additive is not recommended for these solutes, as its ionic strength is too low, leading to a catastrophic deterioration in efficiency when sample concentrations of even a few mg/L are injected.

1. Introduction

Particles that have an impervious core surrounded by a porous shell have been used since the early days of HPLC, with the first consisting of a solid glass beads of 50 μm diameter coated with a thin layer of an ion-exchange resin [1,2]. The good performance obtained was attributed to rapid mass transfer of solutes in and out of the thin porous layer. Commercial versions of such particles for liquid–solid chromatography gave high column efficiencies, but low sample capacities as only a small fraction of the particle volume was porous. Later versions were developed with a thin shell (0.25 μm) but with much smaller particle diameters (5 μm) specifically for the separation of large molecules. Such molecules have only small diffusion coefficients, and thus the structure of such particles supposedly facilitated diffusion in and out of the porous layer [3]. A considerable advance occurred with preparation of C18 particles of overall diameter 2.7 μm with a 0.5 μm porous shell (Halo, Advanced Materials Technology), which showed minimum reduced plate heights (h) of 1.5 [4]. Similarly high efficiencies were reported with a bare silica version of the same material, in the hydrophilic interaction (HILIC) mode [5]. The backpressures generated by these new shell particles were only a little higher than those of 3 μm particles, but yielded efficiencies similar to those of sub-2 μm particles. Indeed, in the HILIC mode, which has the additional benefit of low viscosity, organic-rich mobile phases, shell particle columns of sufficient length could be used to generate over 100,000 plates in reasonable analysis times, with back pressures at the optimum flow velocity that were well within the capacity of conventional HPLC systems («400 bar). There is thus considerable interest in the comparison of the performance of shell and sub-2 μm particles, the latter requiring specialised instruments capable of higher pressures [2,6–9]. Since the commercial development of Halo, alternative shell materials have become available from at least three further manufacturers e.g. Kinetex (Phenomenex),

* Tel.: +44 117 3282469; fax: +44 117 3282904.
E-mail address: David.Mccalley@uwe.ac.uk

0021-9673/$ – see front matter © 2011 Elsevier B.V. All rights reserved.
doi:10.1016/j.chroma.2011.02.068

Ascentis Express (Supelco) and Poroshell (Agilent). Their excellent performance has been attributed to reduced longitudinal diffusion in the smaller porous volume, and reduced eddy diffusion [2]. A strong relationship has been demonstrated between the particle size distribution (which is narrow for shell particles) and the packing quality [10].

Recent research has reported both advantages and disadvantages of shell and sub-2 μm columns. An unusually high plate height was reported at high flow and elevated temperatures for Halo C18 particles [11], although other work did not confirm these findings either for the C18 or the bare silica version of the same material [5,12]. Another factor is frictional heating, a considerable problem in very small particle columns as the power generated is given by the product of pressure and flow rate [13–17]. Heating effects compromise column efficiency, as the mobile phase will travel faster in the central hotter core of the column than at the walls. These effects can be reduced by using a still air heater that approximates to adiabatic conditions, where little heat transfer occurs between the column and its surroundings. In contrast, very poor results are obtained with the column immersed in a water bath, as the column wall is efficiently cooled to the bath temperature due to the higher thermal conductivity of water compared with air. Frictional heating increases with increasing column length and with decreasing particle size, as both increase the back pressure. Detailed mathematical models have been proposed to estimate the temperature profile in the column [18], but it is still difficult to predict the exact effects of this profile on column efficiency. Recent results indicate that frictional heating effects are of less significance for shell particles, because the thermal conductivity of these particles is greater than for totally porous particles [19]. However, the influence of different column dimensions, and different stationary/mobile phases on this effect have not been investigated in detail.

Overload of the stationary phase is an important consideration for ionised compounds in RP separations [20]. With the widespread use of so-called Type B columns made with pure silica, overloading is likely to be the major cause of poor peak shape for acids and bases, as interactions with ionised silanol groups are minimised on these low acidity packings by using low pH mobile phases that suppress their ionisation. The exact mechanism of overload of ionised compounds is still obscure. One view considers that the surface of a Type B RP column consists of a small number of strong sites (e.g. undissociated silanols) that are easily overloaded, together with a much larger number of weak sites that exist at the interface of the bonded layer and the bulk mobile phase [21]. Alternatively, the easy overload of ionised compounds could be due to repulsion of solute ions of the same charge on the surface, giving rise to exclusion effects from the column pores [22,23]. No studies have been published on the overloading of either sub-2 μm or shell particles with ionised solutes. While the porous volume of Halo particles represents 75% of the total volume of the particle, the newer Kinetex particles have a 0.35 μm shell with a 1.9 μm solid core, giving a smaller fraction of porous material in the particle (61%). Clearly, the reduction in the porous volume should reduce the sample capacity of shell particles. Studies have shown that the resolution given by shell particles should increase as the thickness of the porous layer is decreased, as long as the mobile phase strength is reduced to maintain the same k [24]; however, loadability would be reduced. Overload problems are likely to be more severe for both sub-2 μm porous as well as shell particles, due to the very high efficiencies produced by both types of column. This factor will concentrate the sample in a much narrower band than is the case for larger particle, lower efficiency columns. Overload for ionised compounds is strongly dependent on the ionic strength of the mobile phase [21,23]. However, no comparisons of the effect of common buffers used for HPLC with UV detection (e.g. phosphate) and volatile buffers suitable for HPLC with MS detection (e.g. ammonium formate) on overloading have been made.

The aim of the present study was the further practical evaluation of performance as a function of flow and of sample load on these two new types of column, to aid the choice of the optimum approach for a given separation.

2. Experimental

Most experiments were performed on an ultra-high-pressure liquid chromatograph (UHPLC) from Waters (Milford, MA, USA) including Empower data handling, binary solvent manager, photodiode array (PDA) ultraviolet (UV) detector (500 nL flow cell), and sample manager/injector valve using the partially filled loop method (nominal loop volume 5 μL) with needle overfill. The actual loop volume measured by the instrument was 6.75 μL. Sample volumes injected never exceeded 75% of the loop capacity in accord with the recommendations of the manufacturer. The data collection rate was 80 Hz (fast filter, 0.025 s). Data for the Knox curves on the 0.46 cm shell columns were obtained on a modified conventional HPLC (Model 1100, Agilent, Waldbronn, Germany) with Chemstation, UV detector (1 μL flow cell), and Rheodyne 7725 valve (5 μL injections). The fastest data collection rate available on this instrument (14 Hz, response time < 0.12 s) was invariably used. Connections were made with minimum lengths of 0.012 cm i.d. tubing to minimise extra-column band spreading. With large diameter columns (10 × 0.46 cm i.d.), the loss of efficiency for solutes of appreciable k ($k > 2$) was of the order of only a few % on the modified HPLC instrument, necessitating only very small corrections for system band broadening [12]. The column temperature was maintained at 25 °C in both instruments. At least duplicate sample injections were made. The columns used were Halo C18 (10 × 0.46 cm i.d., 2.7 μm particle size), from AMT (Wilmington, USA), Kinetex C18 (5 and 10 × 0.46 cm, and 10 × 0.21 cm i.d., 2.6 μm particle size) from Phenomenex (Torrance, USA), BEH C18 (5 and 10 × 0.21 cm i.d., 1.7 μm particle size) and High Strength Silica C18 (5 × 0.21 cm i.d., 1.8 μm particle size) from Waters (Milford, USA). Acetonitrile (far UV grade) and THF (HPLC grade) were obtained from Fisher Scientific (Loughborough, UK). Acenaphthene, caffeine, naphthalene-2-sulfonic acid, naphtho-[2,3-a]pyrene, phenol and uracil were obtained from Sigma–Aldrich (Poole, UK). System band-spreading was measured by replacing the column with a zero dead volume connector [12]. Diffusion coefficients of the solutes were estimated from the Wilke–Chang equation. The external porosity of the columns was measured by determination of the retention volume of a series of polystyrene standards (Varian/Agilent, Stockport, UK) over the MW range (575–2,851,000) using THF as the mobile phase. Kinetic plots were constructed using an Excel program (Kinetic plot analyser) available from the Vrije Universiteit Brussel [25].

3. Results and discussion

3.1. Knox plots for Kinetex shell particles at different temperatures

Fig. 1 shows Knox plots for naphthopyrene on the Kinetex 10 × 0.46 cm column at 25 °C, 37.5 °C and 50 °C on the modified HPLC system with mobile phases 100, 90 and 85% ACN respectively, together with a plot at 25 °C for the same solute using the UHPLC system. The plots are of the reduced plate height h

$$h = \frac{H}{d_p} \quad (1)$$

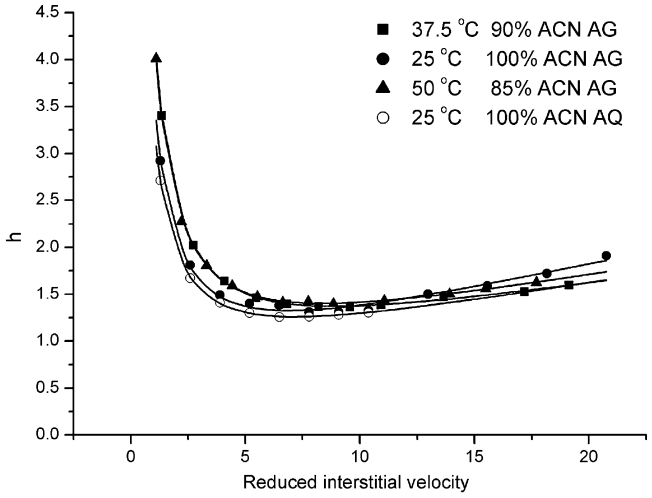

Fig. 1. Plot of reduced plate height vs. reduced interstitial velocity for naphthopyrene on Kinetex C18, 10 × 0.46 cm i.d. Mobile phases as shown. AG = Agilent 1100 (HPLC) instrument, AQ = Waters Acquity (UHPLC). Detection: UV at 290 nm, temperature as shown. Data uncorrected for instrumental band broadening.

against the reduced interstitial velocity

$$\nu_{\text{red,int}} = \frac{Fd_p}{\pi r^2 \varepsilon_{\text{ext}} D_m} \quad (2)$$

where F is the volumetric flow rate, d_p the particle diameter, r the column radius, ε_{ext} the external porosity and D_m the diffusion coefficient of the solute in the mobile phase. Values for the external porosity of the phases, determined by inverse size exclusion chromatography of polystyrene standards, are shown in Table 1. The data in Fig. 1 were not corrected for the instrumental dead volume. k for naphthopyrene was ~3 in 90 and 85% ACN at the temperatures shown; previous work indicated that the loss in efficiency caused by the HPLC instrument should be less than 5% for this column [12]. With 100% ACN, k for naphthopyrene was ~1.5. To reduce further the effects of instrumental volume, injections were made in 85% ACN rather than the mobile phase in this case. The weaker solvent limits the effects of instrument band broadening on the injection. We estimated that the instrumental contribution to band broadening was reduced to ~5%. The success of this approach was shown by the almost exact overlay of the curve obtained using the HPLC and UHPLC systems (up to the maximum flow capability of the latter 2 mL/min and reduced interstitial velocity ~10). The UHPLC system used with this 0.46 cm i.d. column is predicted to cause an even smaller loss of efficiency of around 1% [12]. Theory predicts that all plots should overlay exactly in the absence of unusual effects, as the reduced velocity takes into account the changes in solute diffusion with different temperature and mobile phase viscosity. This overlay is indeed demonstrated in Fig. 1. The plots do not show any unusual upturn in the value of h at high reduced interstitial velocity for this new type of shell particle, as has been reported for Halo shell particles [11], and is instead in agreement with our own previous results for the Halo particles in the RP or HILIC mode [5,12]. Fig. 1 also demonstrates that shell particle columns of 0.46 cm i.d. can be used very successfully on modified conventional instruments, with little detrimental effect on their high efficiency, as long as at least moderate k is used.

Table 1
External porosities of the columns determined by inverse size-exclusion chromatography with polystyrenes.

Column and dimensions	External porosity
Halo C18 10 × 0.46 cm	0.40
Halo C18 10 × 0.21 cm	0.42
Kinetex C18 10 × 0.46 cm	0.39
Kinetex C18 10 × 0.21 cm	0.40
Acquity BEH C18 10 × 0.21 cm	0.36
Acquity BEH C18 5 × 0.21 cm	0.36

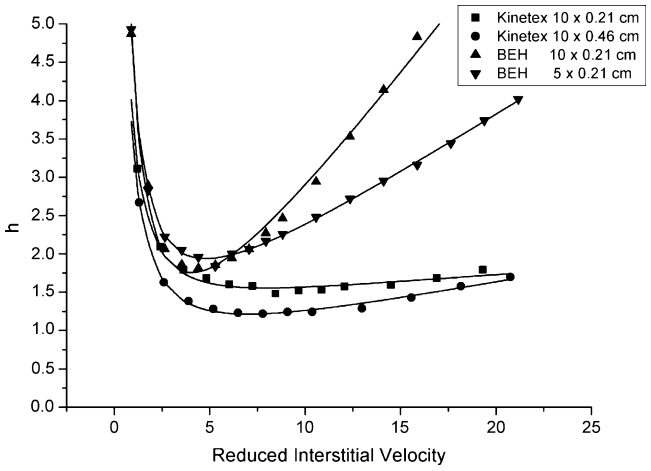

Fig. 2. Plot of reduced plate height vs. reduced interstitial velocity for naphthopyrene on sub-2 μm BEH C18 and Kinetex 2.6 μm C18 columns of various dimensions. Mobile phase 100% ACN, data corrected for instrumental band broadening. Temperature 25 °C. UV at 290 nm.

3.2. Knox plots for shell and sub-2 μm porous particle columns of different dimensions and with different mobile phases

Fig. 2 shows reduced plots for naphthopyrene with pure ACN as the mobile phase at 25 °C for 10 cm Kinetex C18 columns of 0.21 and 0.46 cm i.d. together with 5 and 10 × 0.21 cm BEH C18 columns. In Fig. 2, all data were corrected for the instrumental dead volume. The minimum reduced plate height h_{min} for the 0.46 cm shell column was only 1.2, similar to the values found by others, even for "real-life" compounds such as steroids or peptides [6,24–26]. Around the optimum velocity, the performance of the larger bore shell column is clearly better than that for the narrower bore column (h_{min} = 1.5), suggesting there are some packing issues with the latter. Similar results have been reported elsewhere [6]. Inferior performance of the narrower bore Halo C18 columns has also been noted [12]. At higher flow velocity however, the curve for the 0.21 cm column remains extremely flat whereas h for the 0.46 cm i.d. column rises very slightly, such that the curves intersect at $\nu_{\text{red,int}} \sim 20$. These results suggest that frictional heat dissipation occurs even more readily from the narrower column, reducing the radial temperature gradient. In comparison, h_{min} for both BEH columns was around 1.8. However, the 10 cm BEH column showed a steep rise in h with increasing flow rate, with the 5 cm column demonstrating a considerable if lesser increase. The contribution of mass transfer to h for these very small particle columns has been shown, through detailed practical and theoretical studies of Gritti and Guiochon, to be very small [2]. It seems very likely that the steep rise in the curve for the BEH particles is attributable to frictional heating. Taking values for the thermal conductivities of non-porous silica, liquid octadecane, and liquid acetonitrile as 1.40, 0.15, and 0.20 W/m/K, respectively, Gritti and Guiochon estimated the thermal conductivity of BEH-C18 immersed in pure liquid acetonitrile as 0.31 W/m/K, compared with 0.69 W/m/K for the Kinetex columns [19]. Thus, the higher thermal conductivity of the shell particle provides better dissipation of the frictional heat generated. Furthermore, more power is generated at the higher pressure of operation of the sub-2 μm column, by considering the equation [16]:

$$\text{Power generated} = \text{pressure} \times \text{flow} \quad (3)$$

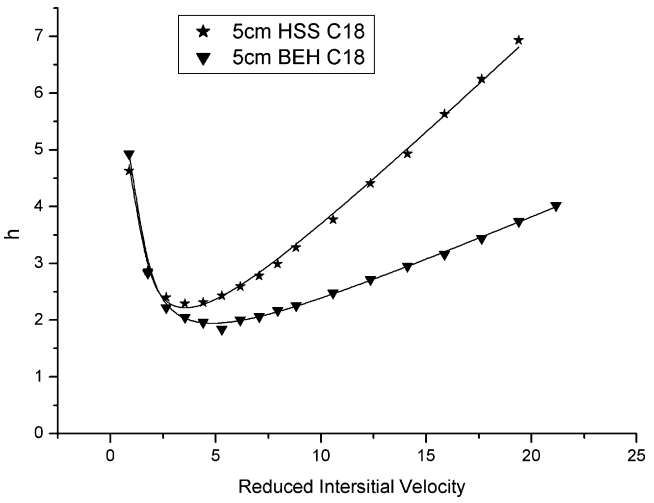

Fig. 3. Plot of reduced plate height vs. reduced interstitial velocity for naphthopyrene on sub-2 μm BEH C18 and high strength silica C18 columns, 5 × 0.21 cm i.d. Other conditions as Fig. 2.

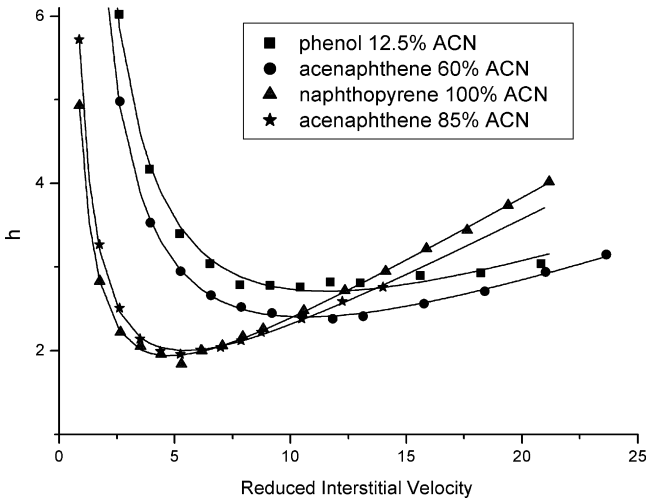

Fig. 4. Plot of plate height vs. reduced interstitial velocity for various solutes with different % ACN in mobile phase. Column 5 × 0.21 cm BEH C18. Data corrected for instrumental band broadening. Other conditions as Fig. 2.

For the 10 × 0.21 cm Kinetex column, power generated was 0.41 W compared with 1.4 W for the BEH column of the same dimensions at a constant value of $\nu_{red,int}$ = 20. It has been estimated that heat friction begins to affect column efficiency significantly above 4 W/m, i.e. above 0.4 W for a 10 cm column [17]. Note the power generated at a constant $\nu_{red,int}$ also depends on differences in column particle size, and diffusion coefficient of the test solute, which contribute to the value of $\nu_{red,int}$. The beneficial effects of lower operating pressure and increased thermal conductivity of the packing both contribute to the favourable properties shown by the shell particles at high flow.

As previous experiments noting the effect of frictional heating have been carried out on hybrid inorganic/organic polymer stationary phases (BEH C18) we repeated the same experiment using a high strength silica phase (Fig. 3) to determine if the results were instead due to some unusual feature of the hybrid material. However, the increase in *h* at high velocity was even greater for the pure silica than for the hybrid phase. The power generated at $\nu_{red,int}$ = 20 was calculated as 0.66 W on the hybrid phase compared with 0.60 W for the pure silica phase, the somewhat lower power for the latter being due to the slightly larger particle size (1.8 μm compared with 1.7 μm for the hybrid phase). Clearly the effect is not confined to one type of small particle packing.

If column efficiency at high flow is influenced by radial thermal gradients, then efficiency will be affected by the mobile phase composition, which will influence the power generated (due to the different backpressure necessary to maintain a given flow) and also the mobile phase thermal conductivity and thus heat dissipation from the column. Fig. 4 shows plots of *h* vs. $\nu_{red,int}$ for phenol with 12.5% ACN as mobile phase, acenaphthene with 60 and 85% ACN and naphthopyrene with 100% ACN, using the 5 cm BEH column. Different solutes were chosen to maintain high *k* so that the correction applied to the column efficiency for the instrument dead volume remained small. The molecular volume of naphthopyrene (MW = 302) is about twice that of acenaphthene (MW = 154) according to calculations based on the group contribution approach [27] but the solute is small compared with the pore size of the packings used (pore size of Kinetex 100 Å, BEH silica 130 Å). Using equation 3, the power generated at $\nu_{red,int}$ = 20 for these solutes and mobile phases was estimated and the results are shown in Table 2. The thermal conductivities of pure water and pure acetonitrile at 25 °C are about 0.61 and 0.19 W/m/K [28,29]. The thermal conductivity

Table 2
Power generated in a 5 × 0.21 cm 1.7 μm BEH column in analysis of various solutes at a reduced interstitial velocity = 20, and thermal conductivities of the mobile phase.

Mobile phase % ACN	Power (W)	Thermal conductivity (W/m/K)
100	0.66	0.19
85	0.88	0.31
60	0.62	0.44
12.5	0.86	0.59

of a liquid mixture can be estimated from the equation:

$$\lambda = \lambda_1 y_1 + \lambda_2 y_2 - (\lambda_1 - \lambda_2)(1 - \sqrt{y_1})\, y_1 \quad \text{for} \quad \lambda_1 > \lambda_2 \qquad (4)$$

where λ_1 and λ_2 are the thermal conductivities of the individual solvents and y_1 and y_2 are their mass fractions in the mixture [30,31]. A plot of thermal conductivity for different ACN–water mixtures is shown in Fig. 5 and Table 2 gives the values for the different mobile phases used. It appears that the steepness of the upturn in the plots at high flow velocity is broadly in line with the decrease in the thermal conductivity of the mobile phase. The flattest Knox curve was obtained for phenol in 12.5% ACN which has a thermal conductivity (0.59 W/m/K) three times greater than 100% ACN (0.19 W/m/K) as used for naphthopyrene. Of course, the results are influenced also by the differences in power generated for the different systems. Greater frictional heat is produced by the higher backpressure required to operate the column with 12.5%

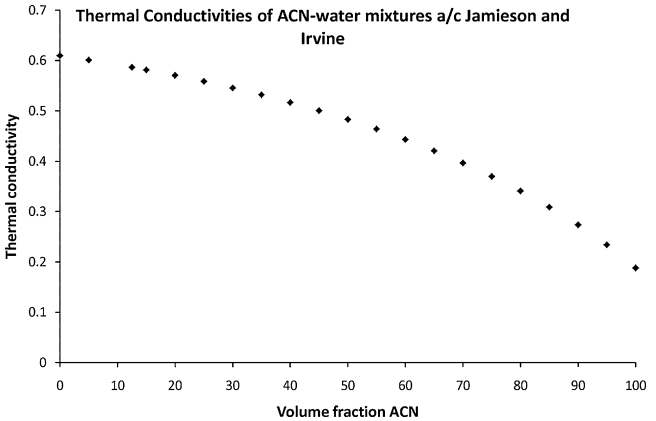

Fig. 5. Thermal conductivities of ACN–water mixtures according to the equation of Jamieson and Irvine [29].

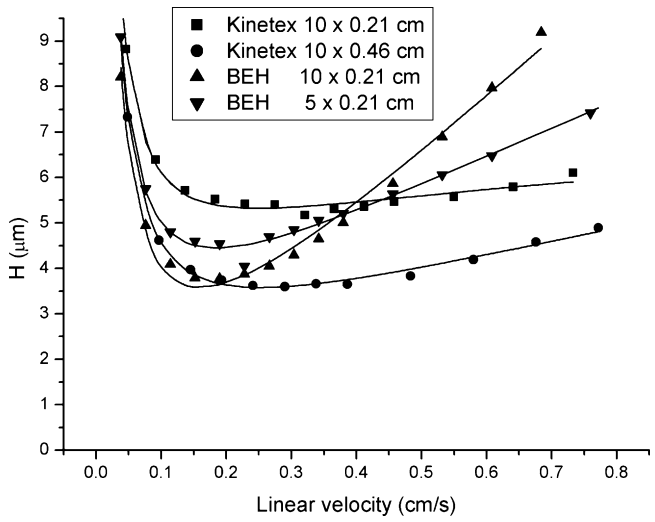

Fig. 6. Plot of plate height vs. linear velocity. Data as for Fig. 2 but uncorrected for instrumental band broadening.

ACN with phenol to give the same reduced interstitial velocity as for naphthopyrene with 100% ACN. The greater power generated for acenaphthene in 85% ACN compared with naphthopyrene in 100% ACN somewhat lessens the effect of the greater thermal conductivity of the former solvent. While caution is necessary in comparison of results for different solutes (different diffusion/different mobile phases), it does appear that the detrimental effects of frictional heating, which are very prominent in 100% ACN, are less important in mobile phases more typically used in RPLC.

Fig. 6 shows the data of Fig. 2 plotted as simple plate height uncorrected for instrument bandspreading against linear velocity. While the trends shown are the same as using the corrected data and reduced parameters, the plots give some idea of the performance that can be achieved in practice on typical HPLC systems. Thus, at the optimum flow velocity the 10 × 0.21 cm sub-2 μm BEH column (operated on the UHPLC instrument) and the 10 × 0.46 cm shell column (operated on the HPLC instrument) gave almost identical efficiencies, albeit at much higher pressure on the former column. At a linear velocity of 0.5 cm/s, the pressure on the BEH column was 446 bar using 100% ACN compared with 194 bar for the Kinetex column. These pressures were corrected for the system pressure by subtracting the pressure generated for the entire system (injector, connecting tubing and detector) with a zero dead volume connector replacing the column. The 10 × 0.21 cm Kinetex shell column (operated on the UHPLC) gave considerably inferior performance to a column containing the same particles but of dimensions 10 × 0.46 cm operated on the modified HPLC system (see Fig. 6), due to a combination of the poorer inherent efficiency of the narrow diameter column (as demonstrated by the data corrected for the instrument dead volume shown in Fig. 2) and the greater effects of instrumental dead volume on chromatographic peaks of lower volume eluted from the narrower bore column. The effects of instrumental dead volume diminish as k increases [12], but the moderate retention of naphthopyrene on the Kinetex column ($k \sim 1.5$) gives rise to a considerable detrimental influence. It is initially surprising that a narrow bore column operated with a state of the art instrument UHPLC instrument shows more detrimental effect of instrumental dead volume than a standard bore (0.46 cm) column operated on a (albeit optimised) conventional HPLC instrument. Finally, while showing smaller frictional heating effects at high mobile phase velocity, the shorter 5 cm sub-2 μm column shows larger plate height at the optimum velocity due to the greater effects of instrument dead volume when considering the moderate k of the solute ($k = 1.9$) [12].

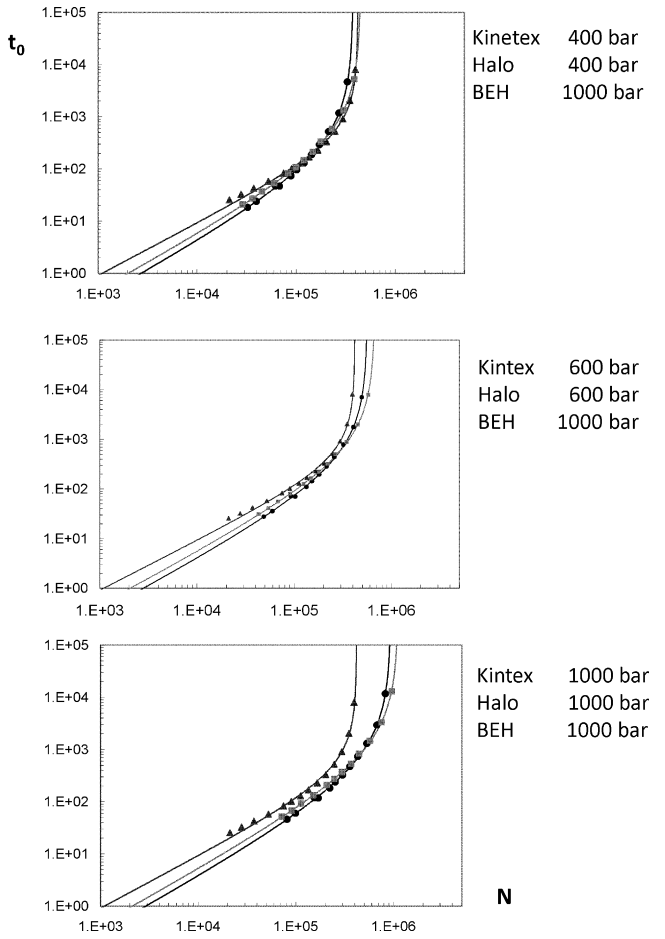

Fig. 7. Kinetic plots of t_0 vs. N for naphthopyrene on 10 × 0.21 cm BEH C18 (triangles), 10 × 0.46 cm Kinetex C18 (circles) and Halo C18 columns (squares) using (a) maximum operating pressures for the shell columns of 400 bar (pressure limit of a conventional HPLC), (b) 600 bar (present upper pressure limit for shell columns) and (c) 1000 bar for all columns. Maximum operating pressure = 1000 bar for BEH in each case.

3.3. Kinetic plots at different pressures

Kinetic plots provide a useful way of comparing the performance of columns that differ in properties such as different particle size and backpressure. In this method, plate height data obtained on a single column are extrapolated to estimate the column efficiency obtainable on a column of length sufficient to generate the maximum operating pressure of the system at a given analysis time, at which point the performance of the column is optimal [32,33]. Simple kinetic plots of the column dead time t_0 vs. the column efficiency N for naphthopyrene (corrected for the instrumental contribution) using pure ACN as the mobile phase at column pressures for the shell particle columns of 400 bar are shown in Fig. 7a, at 600 bar in Fig. 7b and at 1000 bar in Fig. 7c. Calculations were made invariably at 1000 bar for the BEH column. Calculations were based on efficiencies obtained on the wider bore 10 × 0.46 cm Kinetex column (as this gave better performance – see above) and a 10 × 0.21 cm BEH column (note frictional heat dissipation would be much more problematic on a larger diameter column of this type). 400 bar is the maximum pressure available from conventional HPLC systems, 600 bar the manufacturers' current recommended upper pressure limit for the 0.46 cm shell columns (and the maximum pressure for some modern HPLC systems), and 1000 bar the maximum operating pressure of the UHPLC system used, which is also around the mid-range value for these new very high pressure systems. At

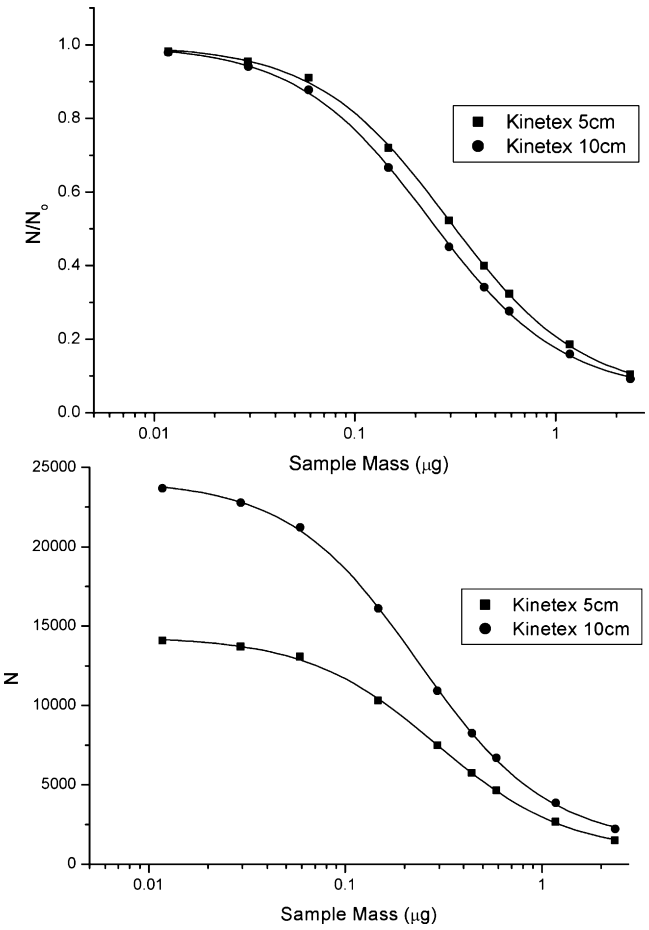

Fig. 8. Plots of efficiency and efficiency as a fraction of limiting (small mass) efficiency vs. mass nortrip for 5 and 10 × 0.46 cm Kinetex C18 columns. Mobile phase 20 mM AF buffer in 35% ACN, 1.0 mL/min. Data obtained on UHPLC instrument.

400 bar, the shell columns show very similar performance to the porous column at 1000 bar for t_0 times of 50–1000 s (Fig. 7a). Note that t_0 times can be simply converted to analysis time using the relationship:

$$t_R = t_0(1 + k) \quad (5)$$

At t_0 = 500 s, the maximum plate number of the BEH, Kinetex and Halo columns was 237,000, 214,000 and 219,000 plates respectively At t_0 < 100 s, the porous column showed a smaller plate number than the shell particle columns, attributable to the upturn in the Knox curves at high mobile phase velocity caused by frictional heating. The Kinetex column gave more plates at small t_0 times than the Halo column, whereas at t_0 > 1000 s the Halo column generated the most plates. These results for the shell particles correspond with the smaller particle size of the Kinetex phase but the higher back pressure that it generates compared with the Halo column, allowing longer columns of the latter phase to be used at the maximum designated operating pressure [34]. For naphthopyrene, it is clear again that the use of shell particles on conventional instruments will give roughly the same performance as sub-2 μm porous particles on ultra-high pressure instruments for commonly used analysis times.

Fig. 7b shows the advantages of operating the shell columns at their maximum pressure (600 bar). At t_0 = 500 s, the maximum plate number of the BEH, Kinetex and Halo columns is 237,000, 278,000 and 275,000 plates respectively At t_0 > 500 s, the performance of the shell particles is further improved. The plots indicate the possibility of using much longer columns than is possible with the small particle porous column, within the pressure limitation of the calculation. The use of UHPLC instruments with shell columns is advantageous not only to allow the operation of longer columns, but also because such instruments reduce still further the effects of the instrument on the efficiency of the (0.46 cm i.d.) column.

While the maximum operating pressure recommended by the manufacturers for both types of shell particle columns is 600 bar, Fig. 7c also shows the potential benefits of using such columns at 1000 bar. At the time of writing, we are not certain as to the reasons for this lower maximum operating pressure whether these are hardware considerations or considerations of packing stability at very high pressures. It should be stressed that these results are hypothetical, as these columns are not designed for use at 1000 bar, and there may be safety implications of such misuse. For t_0 = 500 s, the maximum plate number of the BEH, Kinetex and Halo columns at 1000 bar is 237,000, 371,000 and 353,000 plates respectively. As expected, there would be further advantages in the operation of the shell particles above their present maximum pressure limit on instruments capable of higher operating pressures. Note in the kinetic plots for the shell particles that increasing pressure benefits analyses where larger numbers of plates are desired, moving the curves further to the right in the plot. In this region, long columns are used at the maximum operating pressure; an increase in allowed pressure allows the use of velocities closer to the optimum velocity, where the detrimental effect of axial diffusion (van Deemter B term) is lessened. In contrast, an increase in pressure has very little effect on the lower left hand region of the kinetic plot. Here, the optimum column length is short enough to allow use of a velocity that is already situated in the C term dominated region of the curve, where the available pressure is already more than enough for operation at its kinetically optimum conditions (in a column that is exactly long enough to yield the optimum velocity at the maximum pressure). Thus, there is very little effect of increasing the pressure from 400 to 1000 bar on the performance of any of the columns for fast analysis (the lower left hand regions of Fig. 7a–c are very similar). The interpretation of kinetic plots is explained in more detail by the originators of this methodology elsewhere [34].

3.4. Overload effects

For the study of overload, the strong base nortriptyline (nortrip, pK_a = 10.3) and the strong acid naphthalene-2-sulfonic acid (2-NSA, pK_a 0.61) were chosen, as they should remain completely ionised under the conditions of the experiment. The Kinetex C18 shell column was selected for the study as this has a smaller volume fraction of porous material than Halo C18. A previous study showed good loadability of ionised bases on the Halo unbonded silica col-

Table 3
pH, ionic strength and buffer capacity for buffers used.

	Concentration (mM)	pH	Ionic strength	Buffer capacity (mM/L. pH)
Ammonium formate	20	3.00	21.2	45.5
Potassium phosphate	20	3.00	21.2	7.6
Formic acid 0.1% (v/v)	26.5	2.68	2.2	9.7

umn in the HILIC mode [5]. However, HILIC silica columns show much less deterioration in efficiency as sample load is increased for these solutes compared with RP columns of the same dimensions [35]. It may be that the strong contribution of ionic interactions in HILIC causes this effect by providing additional sites to accommodate solute ions. The 10 × 0.46 cm Kinetex column was selected for the study (as it provided higher efficiency than the narrower bore column) and compared with the 10 × 0.21 cm BEH column. All overloading experiments were performed on the same instrument (UHPLC). A 4.8 μL injection was made for the Kinetex column compared with a 1 μL injection for the BEH phase, these volumes corresponding to the ratio of the volume of packing material in each column. The injector was carefully calibrated with the same column in place to determine the correct nominal volumes to inject to achieve an exact 4.8:1 ratio. This same factor also affects UV detection proportionally, and the same peak area is expected from the narrow bore column by injecting a volume 4.8 times less than for the 0.46 cm column. The % ACN was adjusted to establish the same k (3.75) for each solute with each column and mobile phase. Use of constant k facilitates comparison of results, as the fraction of the injected sample that is associated with the stationary phase at a given instant is given by $k/(1+k)$. A relatively large value of k was chosen as small variations in k should have little impact on overload. Furthermore, only small corrections (<10%) for the instrumental bandspreading contribution caused for the 10 × 0.21 cm column were necessary. As all overload experiments were performed on the UHPLC system, no corrections were necessary for the 10 × 0.46 cm i.d. Kinetex column.

Table 4
N_0 (limiting column efficiency for small sample mass) and $C_{0.5}$ (solute concentration giving half limiting column efficiency) for different columns, solutes and buffers.

Column	% ACN	Solute	Buffer	N_0	$C_{0.5}$ (mg/L)
Kinetex C18	35.0	Nortriptyline	Amm. Formate	24,200	48
	34.0		K phosphate	24,900	48
	32.0		Formic acid	18,700	5
BEH C18	36.8	Nortriptyline	Amm. Formate	25,600	85
	36.0		K phosphate	25,100	74
	35.4		Formic acid	27,200	7
Kinetex C18	15.5	2-NSA	Amm. Formate	27,100	88
	16.0		K phosphate	24,900	78
	16.7		Formic acid	21,800	11
BEH C18	16.0	2-NSA	Amm. Formate	26,500	141
	16.5		K phosphate	21,400	126
	16.0		Formic acid	21,300	17

The change in column efficiency with sample load can be characterised by two parameters: the limiting plate count N_0 and the sample loading capacity $\omega_{0.5}$ [36]. The limiting plate count is the plate count that should be observed when the amount of sample injected is so small that a linear isotherm pertains. The sample loading capacity is the sample load that leads to a plate count half the value of N_0. It can also be expressed as a concentration $C_{0.5}$ in mg/L that gives rise to a loss of half of the efficiency. As the injection vol-

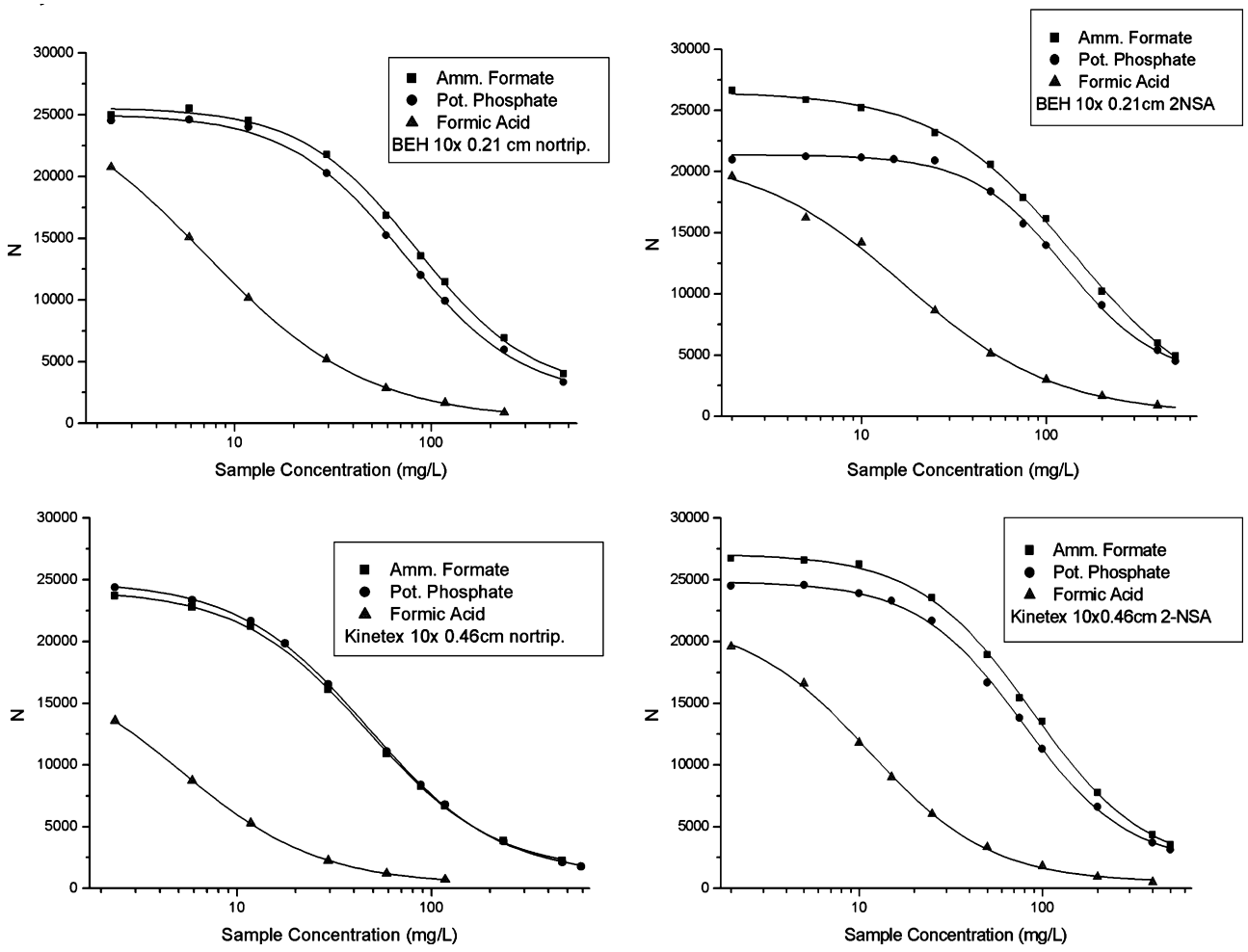

Fig. 9. Plots of efficiency vs. solute concentration for nortrip and 2-NSA on 10 × 0.46 cm Kinetex C18 and 10 × 0.21 cm BEH C18 using 20 mM AF, pH 3, 20 mM PP, pH 3 and 0.1% (v/v) FA in admixture with ACN. ACN concentration was adjusted to maintain k at 3.75 with constant buffer concentration (see Table 4). Flow rate 1.0 mL/min for 0.46 cm i.d. and 0.25 mL/min for 0.21 cm i.d. columns.

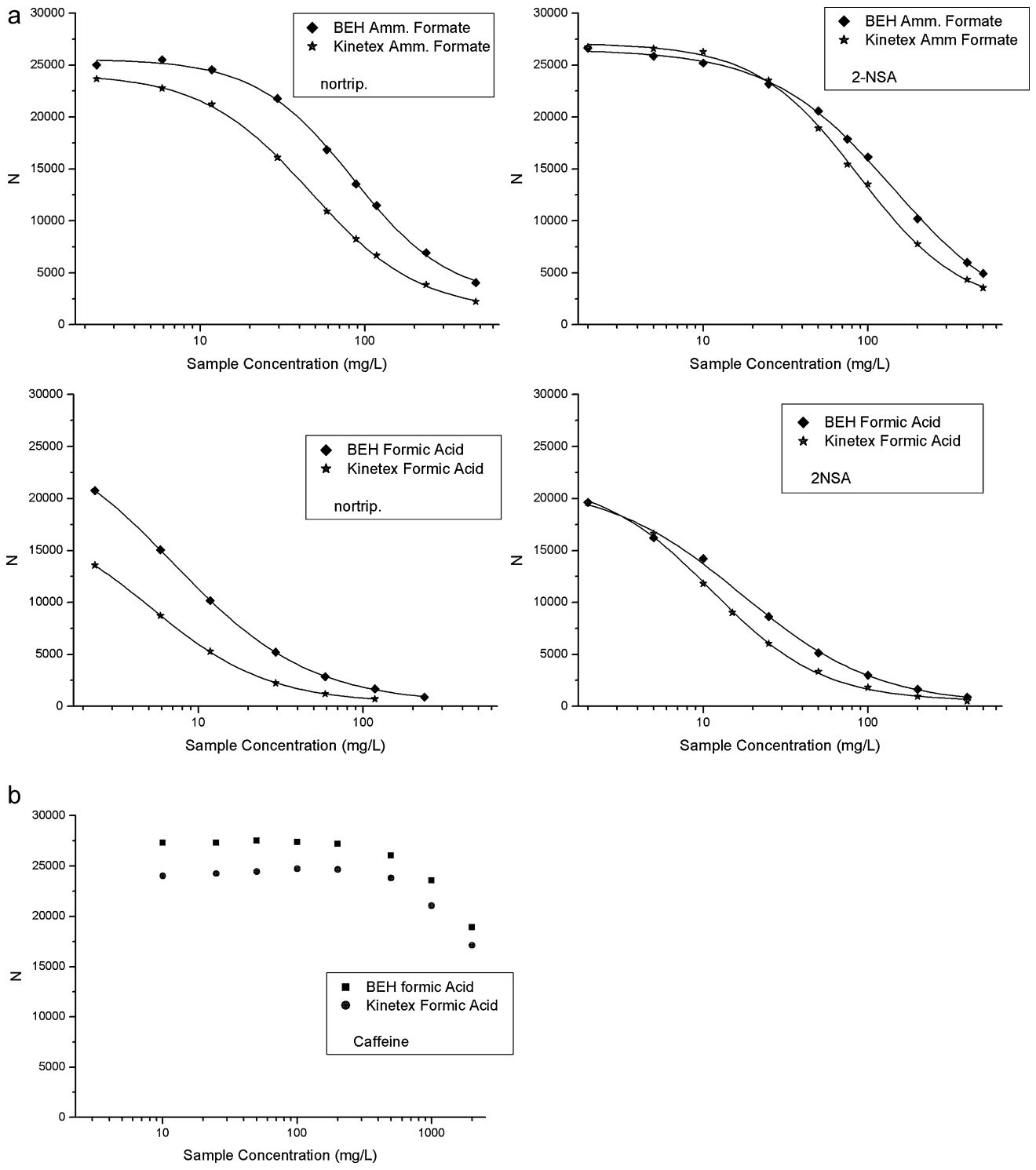

Fig. 10. (a) Plots of efficiency vs. solute concentration as for Fig. 9 but comparing column performance for same solute and buffer. (b) Plots of efficiency vs. solute concentration for caffeine on BEH C18 column (9.2% ACN) and Kinetex column (10% ACN) in 0.1% aqueous FA.

umes were scaled, $C_{0.5}$ values for columns of different i.d. can be compared directly.

Fig. 8 shows the variation in column efficiency with sample mass of nortrip using 5 or 10 cm Kinetex C18 columns in conjunction with ACN–ammonium formate buffer pH 3. The variation of the normalised column efficiency N/N_0 is seen to be largely independent of column length (Fig. 8). Obviously, batch-to-batch variations in the packing, and differences in the packing density of columns could explain the differences shown. Fig. 8 also shows the variation of the absolute efficiency with sample mass for the two columns. While the longer column gives rise to peaks of larger volume at the column exit which reduces overloading, the higher efficiency of this column increases the influence of overloading. These effects cancel out. This result is also predicted by the equation [37]:

$$W_{\text{base}}^2 = \frac{16t_0^2(1+k_0)^2}{N_0} + \frac{6t_0^2k_0^2w_x}{w_s} \quad (6)$$

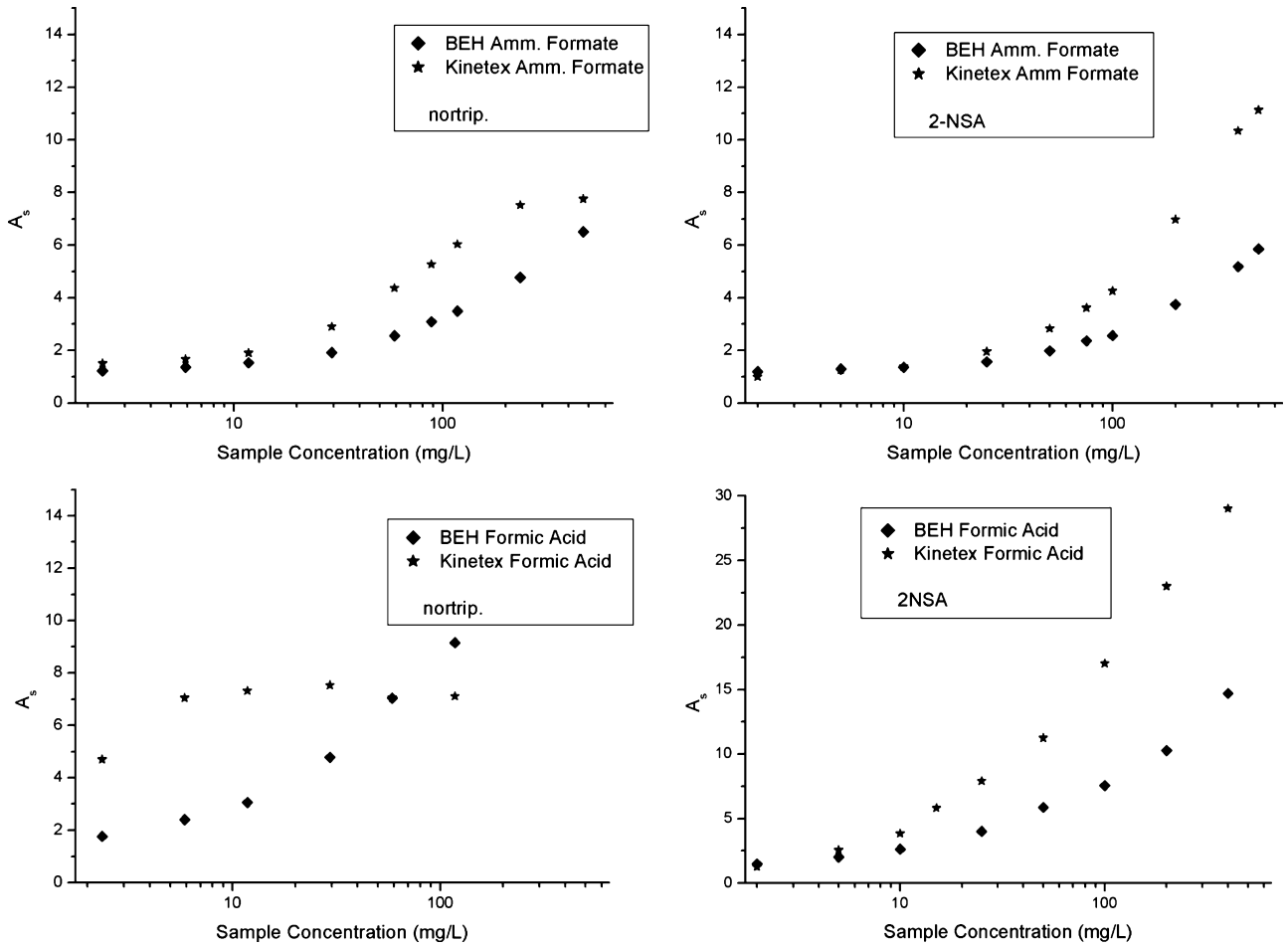

Fig. 11. Asymmetry factors for nortrip in AF and FA buffers as a function of sample concentration. Other conditions as Fig. 9 and Table 4.

where W_{base} is the peak width at base, w_x is the sample mass, t_0 is the column dead time, k_0 and N_0 is the retention factor and column efficiency of a very small sample mass (non-overloaded peak), and w_s the column saturation capacity. Note that the saturation capacity calculated in this way may correspond to the saturation capacity of an important population of scarce strong sites, which dominate the performance of the column, but ignore the loading of the plentiful weak sites, which are only filled afterwards.

Overloading was compared for both nortrip and 2-NSA on the BEH and Kinetex phases in 3 different buffers. Ammonium formate (AF, 20 mM concentration) is a volatile buffer commonly used in LC–MS; potassium phosphate (PP, 20 mM) is commonly used with UV detection; formic acid (FA, 0.1% v/v, ~20 mM), is also very commonly used for MS detection. Table 3 indicates the properties of these buffers. Fig. 9 shows the effect of the nature of buffer on the column efficiency for each solute on the totally porous and shell particle columns. Table 4 shows values of N_0 and $w_{0.5}$ for each column, solute and mobile phase and obtained by fitting a sigmoidal curve to the results. Using the AF or PP buffers, both columns show high values of N_0, typically around 25,000 plates for the basic and acidic solutes. With these buffers, N_0 could be achieved experimentally with the injection of the smallest sample concentration investigated (~2 mg/L), which gave adequate S/N for measurement of the plate count. There was only a small difference in $C_{0.5}$ for these two buffers using either the acidic or basic solute, with AF generally giving slightly better results than PP. For example, for nortrip $C_{0.5}$ was 85 and 74 mg/L respectively for formate and phosphate using BEH C18; for 2-NSA $C_{0.5}$ was 88 and 78 mg/L respectively using Kinetex C18. The volatile buffer is thus an excellent substitute for involatile phosphate for use in LC–MS. Overloading is related to the ionic strength of the buffer [20,21,23]. If overloading is caused by repulsion of ions of the same charge on the phase surface, then increased buffer concentration should assist in screening solute ions from one another. In contrast, the dual site model proposes that increased ionic strength causes increased salting out of sample ions on the weak sites [21]. Whatever the cause of overloading, the similar ionic strength of the formate and phosphate buffers explains the similar results. The most striking feature of Table 4 however, is the extremely low values of $C_{0.5}$ for both columns with these charged solutes, even using the most favourable buffers. For example, injection of a solution of concentration only 85 mg/L for nortrip and 141 mg/L for 2-NSA gives rise to serious degradation in the performance of the BEH C18 (loss of half the efficiency) using formate buffer. In the same buffer, $C_{0.5}$ for Kinetex C18 is 48 and 88 mg/L for nortrip and 2-NSA respectively, these being around 60% of the values for the totally porous column. This result seems reasonable as the surface area of the BEH C18 and the porous part of the Kinetex C18 columns are rather similar at 181 [38] and 211 m^2/g [39] respectively. In this case, it is reasonable to expect the loading capacity to be in line with the fraction of the column volume which is porous. For FA, the results were considerably worse. Values of N_0 in Table 4 were derived from extrapolation of the sigmoidal curve, as the limiting plate count could not even be achieved with injection of the smallest solution concentrations used experimentally (~2 mg/L, see Fig. 9). The ionic strength of FA (Table 3) is about an order of magnitude lower than that of the other buffers, and thus results in much lower $C_{0.5}$ values. Clearly the buffer capacity of FA

and phosphate is not an issue with these experiments, as that of FA is slightly greater than pH 3.0 phosphate buffer, while still giving considerably inferior loading properties. Comparison of the performance of the two columns in the same mobile phase for the same solute is facilitated for the most and least favourable mobile phases (AF and FA respectively) in Fig. 10a. Fig. 10b shows also a plot of efficiency vs. sample concentration for caffeine (pK_a 0.5) in the FA mobile phase, where it is essentially uncharged. Only a minor loss in efficiency is indicated for either column even with injection of a 1000 mg/L solution. Fig. 11 shows the increase in the asymmetry factor (A_s) with solute concentration for AF and FA buffers. Even with AF, perfect peak symmetry ($A_s \sim 1$) was barely achieved for either ionised solute on either column using the smallest injected concentration (2 mg/L). For each column and solute, peak asymmetry increased more rapidly for the Kinetex than the BEH column, in parallel with results for column efficiency. Very large values for A_s were obtained using FA as mobile phase. The apparent stabilisation of A_s at around 7 with nortrip as solute with Kinetex and FA was due to peak distortion. In comparison, the asymmetry of caffeine peaks hardly changed from the optimum value ($A_s \sim 1.0$) until very high concentrations of solute were injected (results not shown).

The poor loading capacity of both sub-2 μm porous and particularly of shell particles is a serious limitation in their application to the separation of ionised compounds. While ionised compounds overload readily even on 5 μm particle size columns, their lower efficiency is advantageous for loading. For example, for nortrip using a 0.46 i.d. XTerra RP 18 column with a similar AF buffer, a value of $C_{0.5}$ of 315 mg/L can be estimated from previous data [35], nearly 7 times larger than that for the high efficiency shell particles and nearly 4 times greater than that for the sub-2 μm porous particles. This 5 μm column had an efficiency of ~7000 plates in a 10 cm length for nortrip compared with ~25,000 plates for the 10 cm columns of the present study. As peak width is inversely proportional to the square root of the efficiency, the predicted effect would be to lower the sample capacity for the shell and sub-2 μm and the shell particle columns by a factor of about 4 and 2 times respectively, somewhat less than the experimental results. However, the 5 μm column was a different material and other factors other than the efficiency (including differences in surface area) will be involved.

A large number of applications use low pH and will suffer from this limitation. It may be alleviated somewhat by the use of buffers of higher ionic strength than used in this work [23], although solubility issues may then become problematic, and mass spectrometer sensitivity is reduced. Alternatively, use of hybrid particles at high pH for analysis of bases should be considered seriously, as overloading is greatly reduced when the solute is not ionised [40–42]. The manufacturer claims the BEH phase is stable up to pH 12, whereas the Kinetex phase is recommended for use only up to pH 8 in mobile phases with high aqueous content [38,43]. The loading capacity with FA may also be improved by the use of charge stabilised hybrid columns that have recently been developed [44].

4. Conclusions

Shell particles give excellent efficiency that is maintained even at high flow velocity. No evidence was found for an unusual upturn in the value of h at high values of flow velocity at elevated temperature (up to 50 °C) either for the new type of shell particle studied in the present work (Kinetex), or the original (Halo) particles studied previously [12]. Using data corrected for instrument bandspreading, smaller values of h_{min} were found for 0.46 cm compared with 0.21 cm i.d. shell columns, which can be attributed to packing difficulties with the narrow bore columns. However, 0.21 cm shell columns give even flatter Knox plots, due to more efficient heat dissipation. In comparison, sub-2 μm porous particles showed a rapid increase in h as flow is increased above the optimum due to frictional heating of the packing in some mobile phases. Clearly, part of this effect is due to the higher operating pressures of these small particles. However, an important contribution is the reduced thermal conductivity of this material compared with the shell particles, as has been proposed by Gritti and Guiochon [19]. The effect was demonstrated in the present work for both hybrid silica and pure silica phases. However, the effect was considerably moderated with mobile phases of higher aqueous content and therefore increased thermal conductivity compared with pure ACN. When considering data uncorrected for instrumental band broadening, the practically attainable efficiencies for narrower bore columns of both types (shell and totally porous) are further reduced, due to the effects of the dead volume of even the most modern commercial instruments.

Under the constraints of a conventional system (P_{max} = 400 bar) the performance of shell particles is roughly equivalent to that of sub-2 μm particles on a typical UHPLC (P_{max} = 1000 bar). Conventional instruments modified to reduce their instrumental dead volume (e.g. Agilent 1100) perform well with 0.46 cm i.d. shell columns, as long as at least moderate k is used. Kinetic plots showed that use of shell particles at 600 bar (their present maximum recommended operating pressure) has considerable benefits, as longer columns could be used at this maximum pressure. These benefits increase further if the pressure limitation could be increased to 1000 bar. Thus the operation of shell columns on UHPLC instruments may be preferred, and the minimised instrumental volume typical of such instruments is a further advantage. Nevertheless, high efficiency 0.21 cm i.d. columns operated on a typical UHPLC instrument can show more detrimental effect of instrumental dead volume than 0.46 cm columns operated on a simply modified conventional HPLC.

Overload is a serious problem when analysing ionised acids and bases with both types of column. Using volatile 20 mM ammonium formate buffers, column efficiency was halved by the injection of sample concentrations only 85 mg/L for an ionised base and 141 mg/L for an ionised acid with the sub-2 μm column, even when using small sample volumes (1 μL for a 0.21 mm i.d. column). For the shell phase, the values were even lower-at 48 and 88 mg/L respectively when using a scaled sample volume of ~5 μL for a 0.46 mm i.d. column. The limited sample capacity is attributable in part to the very high efficiency of these columns and consequent concentration of the sample as a narrow band. The lower capacity of shell particles was found to be in line with the proportion of the particle that was porous (~60%). Use of a volatile ammonium formate buffer gave comparable results with a conventional potassium phosphate buffer. Formic acid buffers, however, are not at all recommended as solutions of concentration of only a few mg/L reduce the column efficiency of ionised solutes by half. The analysis of neutral compounds on these columns is in comparison unproblematic. Analysis of ionogenic compounds in their neutral state should be considered instead, providing the column is stable under the required conditions.

Acknowledgement

The author thanks Agilent Technologies and Waters Corporation for some financial support of this work.

References

[1] C. Horváth, B.A. Preiss, S.R. Lipsky, Anal. Chem. 39 (1967) 1422.
[2] F. Gritti, G. Guiochon, J. Chromatogr. A 1217 (2010) 8167.
[3] J.J. Kirkland, F.A. Truszkowski, C.H. Dilks, G.S. Engel, J. Chromatogr. A 890 (2000) 3.
[4] J.J. Kirkland, T.J. Langlois, J.J. DeStefano, Am. Lab. 39 (2007) 18.

[5] D.V. McCalley, J. Chromatogr. A 1193 (2008) 85.
[6] E. Oláh, S. Fekete, J. Fekete, K. Ganzler, J. Chromatogr. A 1217 (2010) 3642.
[7] J.M. Cunliffe, T.D. Maloney, J. Sep. Sci. 30 (2007) 3104.
[8] Y. Zhang, X. Wang, P. Mukherejee, P. Petersson, J. Chromatogr. A 1216 (2009) 4597.
[9] P. Petersson, A. Frank, J. Heaton, M.R. Euerby, J. Sep. Sci. 31 (2008) 2346.
[10] D. Cabooter, A. Fanigliulo, G. Bellazi, B. Allieri, A. Rottigni, G. Desmet, J. Chromatogr. A 1217 (2010) 7074.
[11] F. Gritti, G. Guiochon, J. Chromatogr. A 1169 (2007) 125.
[12] D.V. McCalley, J. Chromatogr. A 1217 (2010) 4561.
[13] A. de Villiers, H. Lauer, R. Szucs, S. Goodall, P. Sandra, J. Chromatogr. A 1113 (2006) 84.
[14] G. Desmet, J. Chromatogr. A 1116 (2006) 89.
[15] D. Cabooter, F. Lestremau, A. de Villiers, K. Broeckhoven, F. Lynene, P. Sandra, G. Desmet, J. Chromatogr. A 1216 (2009) 3895.
[16] H.J. Lin, C. Horvath, Chem. Eng. Sci. 36 (1981) 47.
[17] F. Gritti, G. Guiochon, J. Chromatogr. A 1216 (2009) 1353.
[18] K. Kaczmarski, J. Kostka, W. Zapała, G. Guiochon, J. Chromatogr. A 1216 (2009) 6560.
[19] F. Gritti, G. Guiochon, J. Chromatogr. A 1217 (2010) 5069.
[20] D.V. McCalley, Anal. Chem. 78 (2006) 2532.
[21] F. Gritti, G. Guiochon, J. Chromatogr. A 1217 (2010) 5584.
[22] I. Häglund, J. Ståhlberg, J. Chromatogr. A 761 (1997) 3.
[23] D.V. McCalley, Anal. Chem. 75 (2003) 3404.
[24] K. Horváth, F. Gritti, J.N. Fairchild, G. Guiochon, J. Chromatogr. A 1217 (2010) 6373.
[25] http://www.vub.ac.uk (accessed February 2011).
[26] F. Gritti, G. Guiochon, J. Chromatogr. A 1217 (2010) 1604.
[27] C.R. Wilke, P. Chang, AICHE J. 1 (1955) 264.
[28] Anon., International Association for the Properties of Water and Steam, Berlin, Germany, 2008. http://www.iapws.org/relguide/thcond.pdf (accessed December 2010).
[29] R.J. Hulse, M.W. Anderson, M.D. Bybee, D.D. Gonda, C.A. Miller, J.L. Oscarson, R.L. Rowley, V.W. Wilding, J. Chem. Eng. Data 49 (2004) 1433.
[30] U.N. Gaitonde, D.D. Deshpande, S.P. Sukhatme, Ind. Eng. Chem. Fundam. 17 (1978) 321.
[31] D.T. Jamieson, J.B. Irving, National Engineering Laboratory, Glasgow, Report NEL 567, 1974.
[32] G. Guiochon, Anal. Chem. 52 (1980) 2002.
[33] G. Desmet, LC.GC (Eur.) 22 (2009) 70.
[34] A. Fanigliulo, D. Cabooter, G. Bellazi, D. Tramarin, B. Allieri, A. Rottigni, G. Desmet, J. Sep. Sci. 33 (2010) 3655.
[35] D.V. McCalley, J. Chromatogr. A 1171 (2007) 46.
[36] J. Dai, P.W. Carr, D.V. McCalley, J. Chromatogr. A 1216 (2009) 2474.
[37] L.R. Snyder, G.B. Cox, P.E. Antle, Chromatographia 24 (1987) 82.
[38] Phenomenex product literature.
[39] F. Gritti, I. Leonardis, J. Abia, G. Guiochon, J. Chromatogr. A 1217 (2010) 3819.
[40] N.H. Davies, M.R. Euerby, D.V. McCalley, J. Chromatogr. A 1119 (2006) 11.
[41] J. Samuelsson, A. Franz, B.J. Stanley, T. Fornstedt, J. Chromatogr. A 1163 (2007) 177.
[42] N.H. Davies, M.R. Euerby, D.V. McCalley, J. Chromatogr. A 1178 (2008) 71.
[43] Waters Corporation, product literature.
[44] Waters Corporation, Library Number LITR10167247, 2010.